applied sciences

MDPI

Article

Cyclic Behaviors of Geopolymeric Recycled Brick Aggregate Concrete-Filled Steel Tubular Column

Yanbin Ni [1,2], Xiancheng Liu [3], Yahui Chen [3] and Ruyue Liu [3,*]

[1] School of Management, Xiamen University, Xiamen 361005, China
[2] Yongfu Construction Engineering Group Co., Ltd., Fuzhou 350007, China
[3] School of Civil Engineering, Fujian University of Technology, Fuzhou 350118, China
* Correspondence: lry18pig@163.com

Abstract: Incorporating geopolymeric recycled brick aggregate concrete into steel tubes provides a promising solution to reduce environmental impact of construction and demolition waste. In this paper, geopolymeric recycled brick aggregate concrete-filled steel tubular column (GRBACFST) was developed to improve the environmental sustainability of composite column. Considering the replacement ratio of recycled brick aggregate (RBA), the thickness of the steel tube, type of cementitious materials and the axial compression ratio as the variation parameters, experimental research was performed to explore the cyclic behavior of GRBACFST columns, including the failure mode, bearing capacity, hysteresis curve, ductility and degradation characteristics. Results demonstrated that the failure of GRBACFST columns occurred in the region at column bottom, with the bulge of steel tube and crush of geopolymeric recycled brick aggregate concrete. The proposed GRBACFST columns exhibited favorable hysteretic behaviors with desired bearing capacity, excellent ductility, and energy dissipation behavior, which were enhanced by the increased thickness of the steel tube. The bearing capacity and ductility were reduced with the increase of axial compression ratio, while enhanced with thicker steel tube. Moreover, the degradation of stiffness and strength was more obvious under larger axial compression ratio. The increase of replacement ratio of RBA caused a significant reduction of bearing capacity, while it had few effect on the hysteretic index. It was concluded that the hysteretic behavior of proposed GRBACFST column was not sensitive to the types of cementitious material and geopolymers could serve as an eco-friendly binder for concrete.

Keywords: geopolymer; recycled brick aggregate; cementitious materials; concrete-filled steel tube; cyclic behavior

Citation: Ni, Y.; Liu, X.; Chen, Y.; Liu, R. Cyclic Behaviors of Geopolymeric Recycled Brick Aggregate Concrete-Filled Steel Tubular Column. *Appl. Sci.* **2023**, *13*, 1235. https://doi.org/10.3390/app13031235

Academic Editors: Shehata E. Abdel Raheem, Humberto Varum and Dario De Domenico

Received: 2 December 2022
Revised: 11 January 2023
Accepted: 12 January 2023
Published: 17 January 2023

1. Introduction

Over the past decades, the shortage of natural construction material and social concerns about the environmental issues have been pushing the whole construction industry to seek sustainable and environmentally friendly materials as an alternative to the common concrete material. It has been reported that about 2.4 billion tons of construction waste was produced per year, approximately accounting for 40% of the total urban waste [1]. Most of construction waste was used for landfill, greatly reducing the utilization efficiency of land resources and damaging the natural environment [2]. However, with the industrialization and development of constructional industry, the need for construction material, i.e., concrete, greatly increases, of which the preparation consumes a large proportion of natural aggregates, and it results in great environmental pressure. Therefore, how to reasonably deal with the problem of construction waste accumulation and the depletion of natural stone resource becomes a looming issue. Moreover, another critical issue attributed by the production of construction material relates to the greenhouse effect. It has also been reported that the production of Ordinary Portland Cement (OPC), which usually serves as the common cementitious material for concrete, consumes a large number of natural

resources and produces a large amount of CO_2 emission [3,4]. As a result, it is essential to find an alternative material to the OPC as the cementitious material for concrete. Nowadays, the development of green buildings with low emission of harmful gases and the reuse of construction waste with high efficiency have become hot research issues.

The utilization of recycled crushed wasted concrete rubble from construction waste is achieved by recycled aggregate concrete (RAC) technology, which has been relatively mature in the preparation of RAC as well as its derivatives [5,6]. Considerable research has been carried out on the mechanical properties of recycled aggregate concrete, in terms of the static behavior, dynamic behavior, impact and temperature performance [7–11], durability [12], creep and shrinkage [13,14]. However, micro-cracks produced during the crushing process and weak bond behavior of interfacial transition zone between recycled aggregate (RA) and new cement mortar lead to the relatively poor quality of RAC. It has been demonstrated that the strength of RAC is reduced by about 10–25% [15–17]. Numerous studies on the RAC verified that the application of RAC was an effective solution to the problem of shortage of natural aggregates. The wasted clay bricks from demolished buildings takes up a large proportion of the construction waste, and the reuse of wasted clay bricks could, furthermore, relieve the environmental issues of shortage of natural aggregates. The application of recycled clayed bricks (RBA) is gaining more and more research attention. However, there still exists problems that hinder the promotion of recycled clay bricks, such as lower apparent density, higher water absorption and higher crushing index [18,19]. Several treatment methods were used to reduce the drawbacks of RBA, such as addition of admixtures [20–25]. It was validated that the quality and mechanical strength of crushed brick aggregate were strengthened by pozzolan slurries, and the loss of compressive strength, flexural strength and modulus of elasticity was about 12–25%, 9–22% and 16–30%, respectively, compared with natural aggregate concrete [22].

In recent decades, a new type of cementitious material, geopolymers, has been used to replace the traditional OPC for the preparation of concrete [26,27]. Geopolymer is synthesized by the combination of aluminosilicate materials and high-concentration NaOH solution. It is considered as an eco-friendly binder for concrete, since the aluminosilicate materials (i.e., fly ash and slag) for geopolymers could be extracted from industrial waste, and the preparation could be completed at an ambient temperature with relatively small CO_2 emission [28,29]. Research on the mechanical behavior of geopolymeric recycled aggregate concrete (GRAC) has attracted increasing research attention and it has been validated that the geopolymers serving as the binder for recycled concrete benefits the mechanical properties of RAC [30–33]. Besides, GRAC could develop desired mechanical behaviors. The compressive strength of an optimized RAC with 100% recycled coarse aggregate could reach as high as 43.3 MPa [34] and the inclusion of slag can alleviate the negative effects of RA replacement on peak stress, elastic modulus and energy absorption [35].

Based on the working principle of composite column, constrained materials including steel tube and FRP were used to provide additional confinement to RAC or RBAC [36,37]. The studies [38,39] showed that the utilization of carbon CFRP greatly enhanced the compressive behavior of RAC. It was reported that the strength, deformability as well as durability of RBAC was enhanced with FRP, and the compressive behavior of FRP-confined RBAC was similar to that of FRP-confined NAC [40,41]. The papers [42,43] indicated that the hysteretic behaviors of recycled aggregate concrete-filled steel tube (RACFST) column were similar with conventional CFST column, and the hysteretic behaviors were affected by the replacement ratio of RA, the axial compression ratio, steel tube thickness and steel strength.

Based on this research background, an eco-friendly composite column, geopolymeric recycled brick aggregate concrete-filled steel tube (GRBACFST) column was proposed to further promote the application of GRBAC. For the GRBACFST column, recycled brick aggregates (RBA) were used to replace natural aggregates, while geopolymers were used as binders, and then geopolymeric recycled brick aggregate concrete was incorporated into steel tubes. In this paper, the failure modes and hysteresis behaviors of GRBACFST columns

were studied experimentally, to better understand the mechanism of GRBACFST column under cyclic loading. The influences of replacement ratio of RBA, steel tube thickness, axial compression ratio and cementitious material types were discussed. The research aims to provide some references for the practical application of the GRBACFST column.

2. Test Program

2.1. Test Specimens

Eight half-size GRBACFST columns and three half-size RBACFST columns were prepared and the involved variation parameters included: (1) replacement ratio of RBA (0%, 30%, 50%, 70%, 100%), thickness of the steel tube (4 mm, 6 mm), axial compression ratio (0.05, 0.25, 0.5) and cementitious material (geopolymers, OPC). The clear height for tested specimens was 750 mm, corresponding to slenderness ratio of 39.97, and the detailed parameters were given in Figure 1 and Table 1. The nomenclature for specimens is illustrated as follows: the first two letter "ST" refers the square steel tube; the third letter "G" indicates the cementitious material is geopolymers while "M" refers to OPC; the first number 4 or 6 refers to the thickness of the steel tube, the second number means the replacement ratio of RBA and the last number is the axial compression ratio. Taking STG4-0.5-0.25 as an example, the steel tube thickness is 4 mm, the replacement ratio of RBA is 50% and the applied axial compression ratio is 0.25.

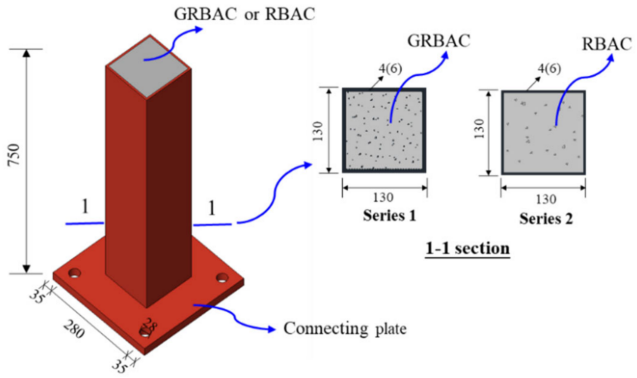

Figure 1. Geometric details of the proposed composite column.

Table 1. Design parameters of specimens.

No.	*D*/mm	*t*/mm	*r*/%	*n*	*N*/kN
STG4-0-0.25	130	4	0%	0.25	320.43
STG4-0.3-0.25	130	4	30%	0.25	298.85
STG4-0.5-0.25	130	4	50%	0.25	292.6
STG4-0.7-0.25	130	4	70%	0.25	294.2
STG4-1-0.25	130	4	100%	0.25	280.73
STG4-0.5-0.05	130	4	50%	0.05	58.52
STG4-0.5-0.5	130	4	50%	0.5	585.21
STG6-0.5-0.25	130	6	50%	0.25	325.44
STM4-0-0.25	130	4	0%	0.25	328.55
STM4-0.5-0.25	130	4	50%	0.25	294.87
STM4-1-0.25	130	4	100%	0.25	275.15

Note: *D* and *t* are the width and thickness of square steel tube, respectively; *r* means the replacement ratio of RBA; *n* is the axial compression ratio, defined as $n = N/(A_s f_y + A_c f_c)$, where *N* is the applied d axial load under test, A_s and A_c are the cross-section area of steel tube and inner concrete, respectively, and f_y and f_c are the yield strength of steel and compressive strength of inner concrete, respectively.

2.2. Material Properties

Table 2 demonstrates the primary properties of steel, which were obtained by a coupon test according to Chinese Standard GB/T 228.1-2010 [44]. GRBAC is prepared with river

sand, crushed brick aggregates, fly ash, slag and alkali activator, where the fly ash, slag and alkali activators were used to prepare geopolymers. The alkali activator was made of Na_2SiO_3 and NaOH solution, where the NaOH solution was prepared by dissolving solid NaOH flakes (98% purity, density 2.13 g/cm^3) in pure water with a constant modulus of 1.4 M. The particle size and gradation of river sand was same with that for recycled brick aggregates, with particle size of 4.75 mm–26.5 mm. The measured water absorption of recycled brick aggregate was 14.97%, higher than river sand of 3.1%; therefore, saturated wetting treatment on brick aggregate was necessary before the preparation of GRBAC. Moreover, 1.5% borax and sucrose were added as retarders to ensure the workability during the preparation of the concrete.

Table 2. Mechanical properties of steel.

B × t (mm)		Yield Strength f_y (MPa)	Ultimate Strength f_u (MPa)	Yield Strain ε_y	Elastic Modulus E_c (N/mm^2)	Poisson's Ratio μ
140 × 4	1	369.5	509.9	0.002466	210,364	0.290
	2	378.4	510.1	0.002651	210,150	0.286
	3	371.8	510.5	0.002620	210,431	0.287
	AVG.	373.3	510.2	0.002579	210,315	0.288
140 × 6	1	308.3	444.9	0.002206	208,532	0.271
	2	299.8	433.9	0.002065	209,368	0.273
	3	310.0	443.2	0.002209	208,134	0.271
	AVG.	306.0	440.7	0.002163	208,678	0.272

Benchmark strength of C50 was selected for ordinary geopolymeric concrete without RBA, and then natural coarse aggregates were replaced with different RBA replacement ratio to prepare GRBAC. It should be noted that the natural coarse aggregates were replaced with RBA by weight. Besides, to explore the influence of different cementitious material, recycled brick aggregate concrete with OPC (RBAC) was also prepared, and replacement ratios of RBA of 0%, 50% and 100% was considered. The mix design for GRBAC and RBAC is outlined in Tables 3 and 4, respectively.

Table 3. The mix design for GRBAC (kg·m^{-3}) and measured strength (MPa).

Specimens	r_{BA}/%	Sols Ratio	Materials						f_{cu}
			Alkali Activator	Fly Ash	Slag	Sand	Stone	RBA	
GRBAC-0	0	0.55	357	487.5	162.5	787	1451	0	55.18
GRBAC-30	30	0.55	357	487.5	162.5	787	1016	435	45.28
GRBAC-50	50	0.55	357	487.5	162.5	787	725.5	725.5	43.05
GRBAC-70	70	0.55	357	487.5	162.5	787	435	1016	42.31
GRBAC-100	100	0.55	357	487.5	162.5	787	0	1451	37.21

Note: sols ratio represents the ratio between the alkali activator and the cementitious materials.

Table 4. The mix design for RBAC (kg·m^{-3}) and measured strength (MPa).

Specimens	r_{BA}/%	Materials					f_{cu}
		Sand	Stone	RBA	Water	OPC	
RBAC-0	0	698	1080	0	180	460	58.73
RBAC-50	50	698	540	540	180	460	43.38
RBAC-100	100	698	0	1080	180	460	34.97

The material property test for GRBAC and RBAC was also conducted according to Chinese Standard GB/T50081-2019 [45]. Three cubic specimens in 150 mm for concrete

with different mix proportion were tested and the results for the average compressive strength of cylinder specimens are also listed in Tables 3 and 4.

2.3. Preparation of Specimens

GRBAC and RBAC were prepared based on the mix design mentioned in Tables 3 and 4. The prepared GRBAC and RBAC were cured under the conditions that the environmental temperature was about 20 ± 2 °C and the humidity was at least 95%, and the curation would last for 28 days. The prepared GRBAC or RBAC was carefully cast into steel tubes step by step and an electrical vibrator was used to ensure the compactness of GRBAC or RBAC during the casting process. All specimens were cured under natural conditions, then the high-strength epoxy mortar was used to fill and polish the surface of concrete before sealing the end. The steel tube was sprayed with red paint and plotted with white grid lines of 25 mm × 25 mm at the bottom region, aiming to facilitate the observation or capture of the damage phenomenon.

2.4. Test Set-Up

The tested specimen was connected to loading cell with a rigid steel plate and fixed to a rigid base with steel anchors and the rigid base was laterally supported with reaction jack and reaction pier to prevent horizontal sway during loading, as shown in Figure 2. The vertical load was applied through hydraulic jack before lateral cyclic loading and then remained constant. Reverse cyclic load was exerted by loading cell, which was connected to MTS actuator fixed on reaction wall. LVDTs were arranged along the height of specimen to record the deformation distribution, as shown in Figure 2b. To record the transverse strain of the outer steel tube, two strain gauges for each side were symmetrically pasted on the surface at the bottom of steel tube. Additionally, the development of the longitudinal strain of the outer steel tube was measured during test, and a total of 24 strain gauges were installed along the surface of steel tube. The layout of strain gauges was presented in Figure 3. Note that in Figure 3, it was specified that the surface far away from loading instrument was Side A, and the opposite surface was Side C. The other two sides were specified in clockwise direction.

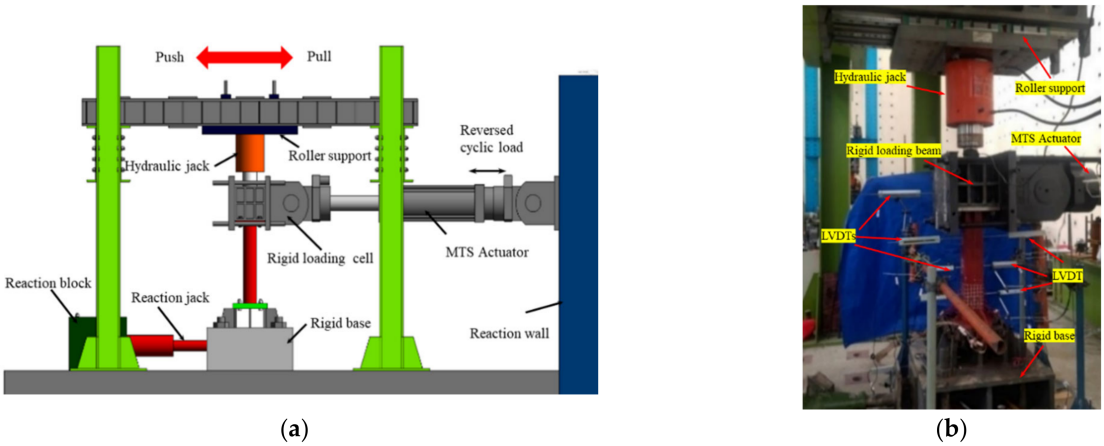

(**a**) (**b**)

Figure 2. (**a**) Diagram of test setup of test setup for reversed cyclic loading; (**b**) specimen photograph of test setup for reversed cyclic loading.

Figure 4 provided the loading history curve for the reversed cyclic load. Before yielding, the force-controlled loading history was adopted, with increment of 0.25 P_{uc}, 0.5 P_{uc} and 0.75 P_{uc} (P_{uc} is the calculated bearing capacity according to ATC-24 [46]), and each loading level was repeated two times. Then, a displacement-controlled loading protocol was used with history curve of Δ_y, $1.5\Delta_y$, $2\Delta_y$, $3\Delta_y$, $4\Delta_y$, $5\Delta_y$ . . . , where Δ_y was the yielding displacement, defined as $\Delta_y = P_{uc}/K_{sec}$, and K_{sec} was the secant stiffness

corresponding to 0.7 P_{uc}. The first three displacement levels (Δ_y, 1.5Δ_y, 2Δ_y) were repeated three times, while the rest was repeated two times. The tested specimen was considered as failed when the bearing capacity degraded to less than 85% of the peak load or the column lost its integrity due to unfavorable serious deformation.

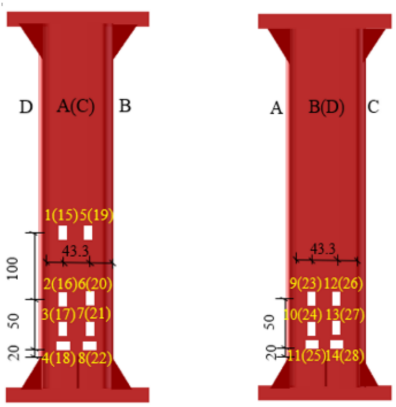

Figure 3. Layout of strain gauges.

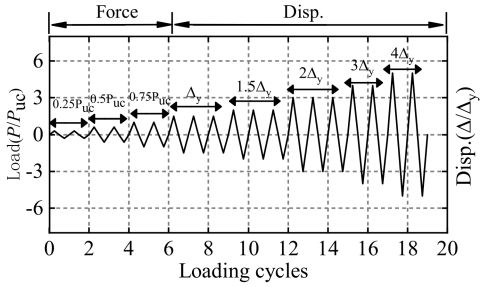

Figure 4. Loading protocol.

3. Test Results and Discussion

3.1. Test Observations and Failure Mode

During the loading process, it was found that all tested specimens exhibited a similar failure process with increasing load and failed with a steel tube bulge at the bottom region or rupture at a corner. For simplification, specimen STG4-0.5-0.25 was taken as an example to elaborate the details of failure process of GRBACFST columns.

At the first loading stage, the load linearly increased with the displacement increasing initially. The specimen remained in elastic state and no obvious damage was found. With the test going on, it was observed that strains in Side A and Side C developed more quickly than in Side B and Side D. The damage evolution was accelerated and more damage was noticed while the test was performed. When displacement loaded up to 1.5 Δ_y–2 Δ_y; a slight bulge in Side A at the column root was captured and specimen STG4-0.5-0.25 achieved the peak bearing capacity when load increased to 3 Δ_y. Then, several visible wrinkles on the steel tube occurred, accompanied with a noise heard when loaded up to 4 Δ_y; it was deducted that the noise was caused by the crack of the inner GRBAC. At the same time, the previous bulge in Side A became more obvious, while the bulge initiated in Side C when loading reversely. With load increasing, the bulge in Side A and Side C alternatively occurred and degradation in bearing capacity was noticed. At displacement of 5.0 Δ_y, the load decreased to about 85% of the peak load and the local buckling of steel tube was aggravated and propagated to adjacent Side B or Side D. The buckling was unable to totally recover when unloaded, leading to obvious residual deformation, and serious debris of red paint at the grid region fell off. It was inferred that plastic hinge formed at the bottom region of column at failure. Besides, to clearly demonstrate the damage of inner

concrete, the steel tube was cut off after the test to obtain the failure mode of the inner concrete. Figure 5 demonstrates the final failure mode and damage of inner concrete for STG4-0.5-0.25.

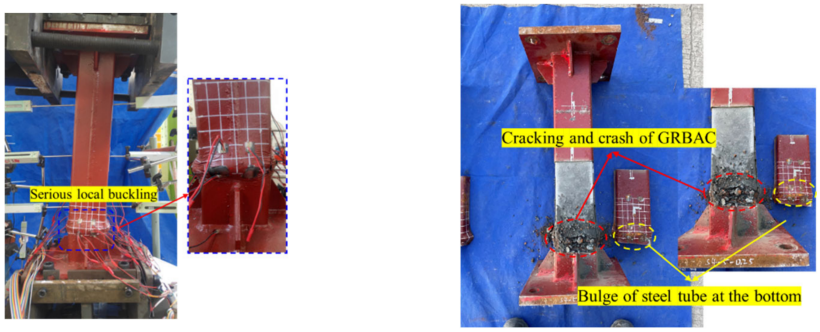

Figure 5. (**a**) Final overall failure mode of concrete for STG4-0.5-0.25; (**b**) damage of inner concrete of concrete for STG4-0.5-0.25.

As mentioned above, all tested specimens exhibited similar failure process and overall failure modes, some differences were also found locally. To clearly demonstrate influence of different parameters, typical local failure for specimens were summarized and presented in Figure 6 and the detailed damage of inner concrete was demonstrated in Figure 7. The damage of GRBACFST columns occurred at the column bottom due to a larger bending moment. When a local bulge or buckling of the steel tube occurred, concrete adjacent to the buckled area was prone to crack under cyclic load, since the confinement effect from the steel tube was impaired. Therefore, the collapse of inner concrete always occurred at the region where serious local buckling of steel tube occurred. The bulge of the steel tube and crash of GRBAC were more serious under larger axial compression due to the P-Δ effect, demonstrated in Figures 6h and 7h.

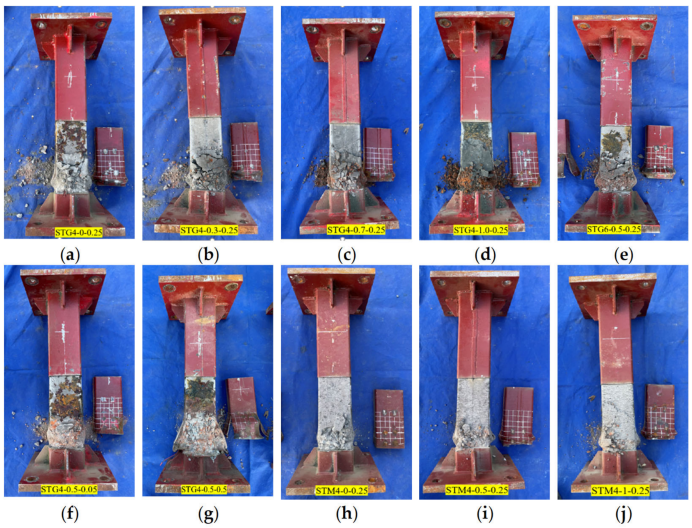

Figure 6. (**a**) Failure of the inner GRBAC for STG4-0-0.25; (**b**) failure of the inner GRBAC for STG4-0.3-0.25; (**c**) failure of the inner GRBAC for STG4-0.7-0.25; (**d**) failure of the inner GRBAC for STG4-1-0.25; (**e**) failure of the inner GRBAC for STG6-0.5-0.25; (**f**) failure of the inner GRBAC for STG4-0.5-0.05; (**g**) failure of the inner GRBAC for STG4-0.5-0.5; (**h**) failure of the inner GRBAC for STM4-0-0.25; (**i**) failure of the inner GRBAC for STM4-0.5-0.25; (**j**) failure of the inner GRBAC for STM4-1-0.25.

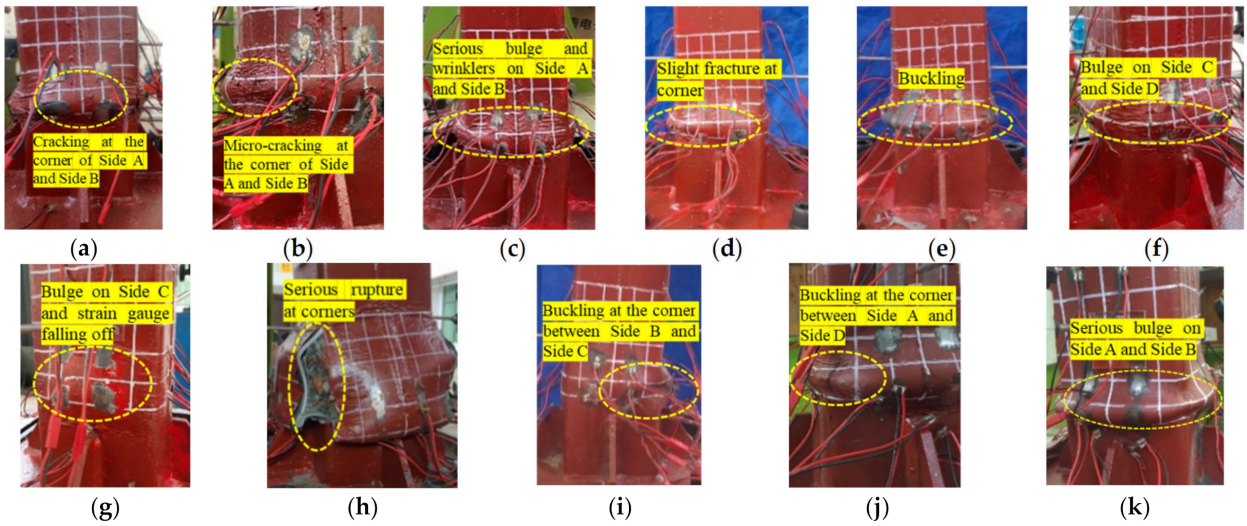

Figure 7. (**a**) Typical local failure of specimens for STG4-0-0.25; (**b**) typical local failure of specimens for STG4-0.3-0.25; (**c**) typical local failure of specimens for STG4-0.5-0.25; (**d**) typical local failure of specimens for STG4-0.7-0.25; (**e**) typical local failure of specimens for STG4-1-0.25; (**f**) typical local failure of specimens for STG6-0.5-0.25; (**g**) typical local failure of specimens for STG4-0.5-0.05; (**h**) typical local failure of specimens for STG4-0.5-0.5; (**i**) typical local failure of specimens for STM4-0-0.25; (**j**) typical local failure of specimens for STM4-0.5-0.25; (**k**) typical local failure of specimens for STM4-1-0.25.

3.2. Hysteresis Curves

Figures 8 and 9 show the hysteresis curves for GRBACFST columns and RBACFST columns, respectively. As seen, all the hysteresis curves were full without an evident pinching effect, implying that the GRBACFST and RBACFST columns all develop desired hysteresis behavior with good energy dissipation capacity. Besides, all tested specimens exhibited approximately symmetric hysteresis behavior in positive and negative direction before failure. The change of variation parameters did not have much influence on the mechanical behavior before reaching peak load, while the difference in degradation behavior was much more evident. It was deduced that the confinement effect from the steel tube offset the impact from different parameters. However, with the occurrence of bulge or local buckling of steel tube, the confinement effect was impaired.

From Figure 8a to Figure 8e, it was found analyzed that the incorporation of RBA improved the degradation behavior, and the bearing capacity decreased with the increase of replacement ratio of RBA. The axial compression ratio had a negative influence on the bearing capacity and deformation capacity (as shown in Figure 8c,f,h), and the degradation of bearing capacity was quicker with larger axial compression ratio. The reason was that it was easier to induce buckling of the steel tube and cracking of the inner concrete under a larger axial load, leading to the premature failure of the cooperation between the steel tube and the inner concrete. Specimens with a thicker steel tube developed a relatively higher bearing capacity and deformation capacity, since a thicker steel tube could provide better confinement and ensure the cooperation between members, leading to slower degradation in stiffness and strength. Compared with the curves in Figure 9, it was found that for specimens with different cementitious material, the hysteretic behavior was analogous with similar bearing capacity and deformation capacity. Additionally, the effect of replacement of RBA on the hysteretic behavior of RBAC columns was close to that of GRBAC columns. It was analyzed that the behavior of proposed GRBACFST columns was mostly determined by the properties of incorporated aggregates and the cooperation between steel tube and inner concrete, rather than the behavior at the interface.

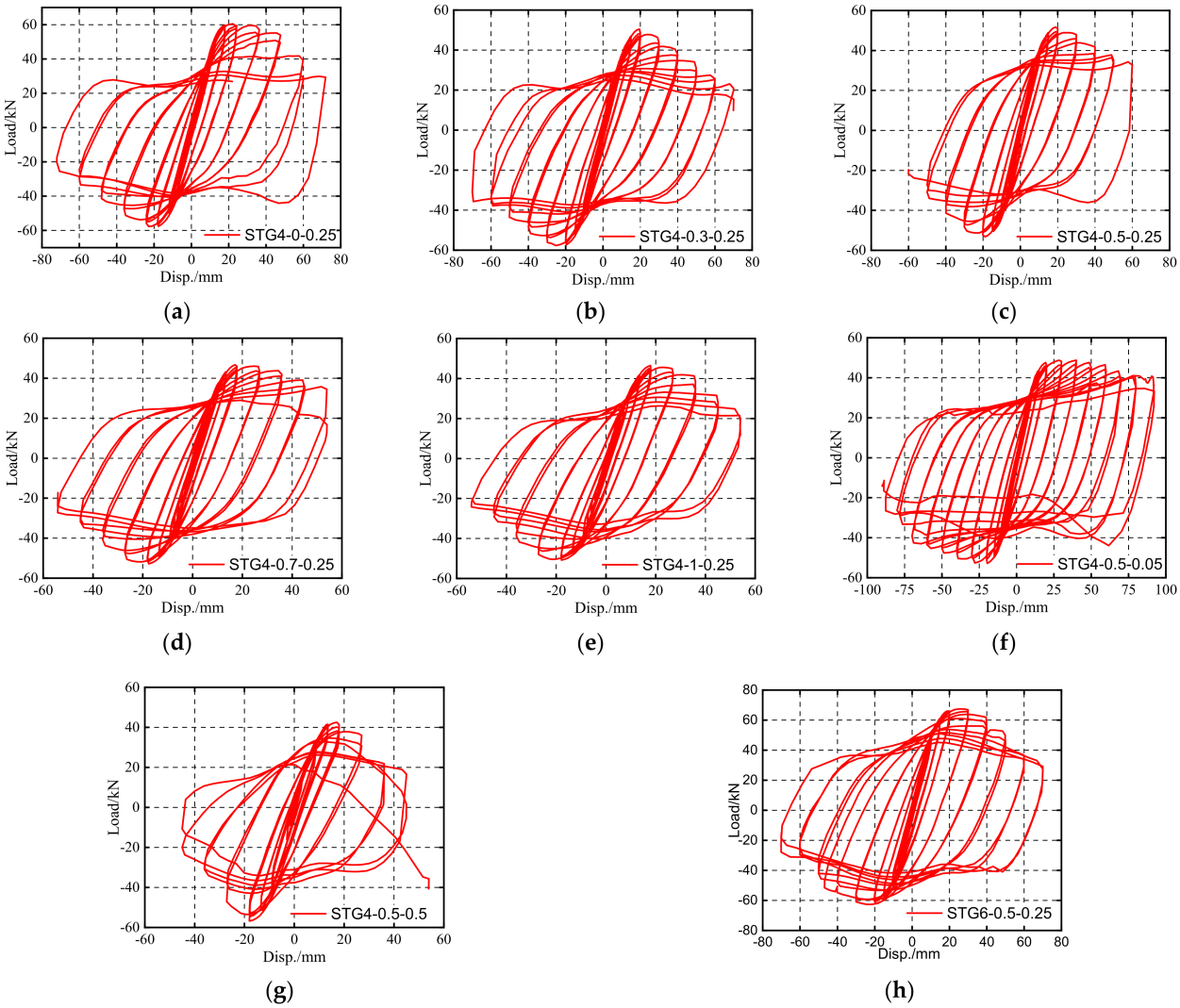

Figure 8. (**a**) Hysteresis curves for GRBACFST columns of STG4-0-0.25; (**b**) hysteresis curves for GRBACFST columns of STG4-0.3-0.25; (**c**) hysteresis curves for GRBACFST columns of STG4-0.5-0.25; (**d**) hysteresis curves for GRBACFST columns of STG4-0.7-0.25; (**e**) hysteresis curves for GRBACFST columns of STG4-1-0.25; (**f**) hysteresis curves for GRBACFST columns of STG4-0.5-0.05; (**g**) hysteresis curves for GRBACFST columns of STG4-0.5-0.25; (**h**) hysteresis curves for GRBACFST columns of STG4-0.5-0.5.

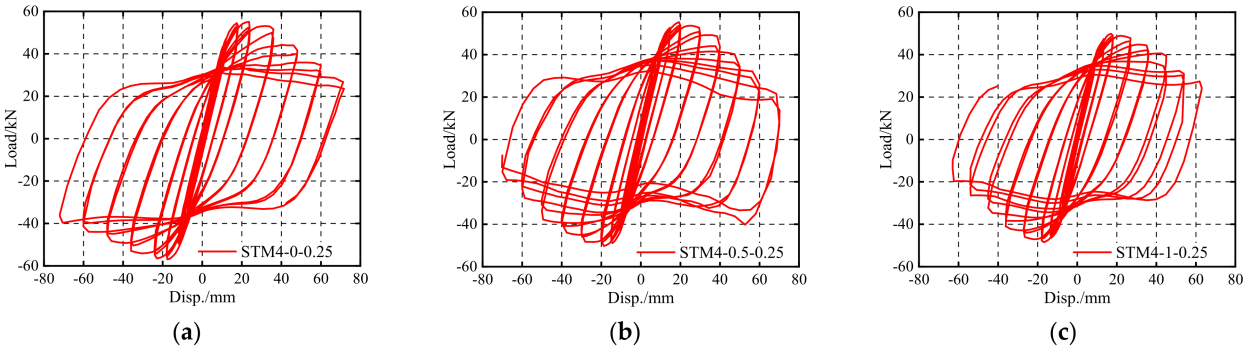

Figure 9. (**a**) Hysteresis curves for RBACFST columns of STM4-0-0.25; (**b**) hysteresis curves for RBACFST columns of STM4-0.5-0.25; (**c**) hysteresis curves for RBACFST columns of STM4-1-0.25.

3.3. Skeleton Curves

Skeleton curves obtained from the successive peak point from hysteresis curve are shown in Figure 10. Initially the displacement linearly changed with an increase of the load, then the growth of load slowed down once yielded. Similar to the discussion in Section 3.2, no evident difference was noticed in the development of load-displacement curve before the yielding of steel tube for different specimens. The bearing capacity and the degradation behavior was significantly influenced by the variation parameters. The mechanical behavior index at the feature point in skeleton curves was analyzed and the corresponding characteristic value is outlined in Table 5.

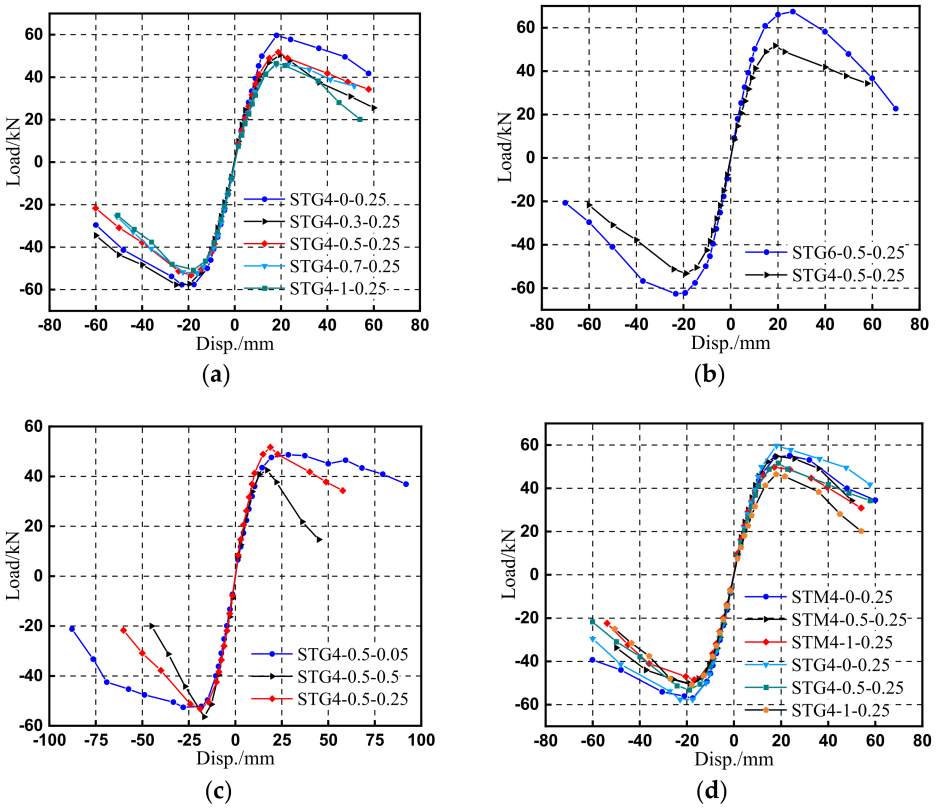

Figure 10. (**a**) Skeleton curves for the replacement ratio of RBA; (**b**) Skeleton curves for the thickness of the steel tube; (**c**) Skeleton curves for the axial compression ratio; (**d**) Skeleton curves for cementitious material.

Table 5. Measured load and displacement at feature points.

Specimen NO.	Direction	Yield Point		Peak Point		Failure Pint		$\mu = \Delta_\mu/\Delta_y$
		P_y/kN	Δ_y/mm	P_m/kN	Δ_m/mm	P_u/kN	Δ_u/mm	
STG4-0-0.25	Pos.	47.88	11.09	59.68	18.05	50.73	44.34	4.0
	Neg.	46.84	10.69	57.7	22.9	49.05	35.28	3.3
	Ave.	47.36	10.89	58.69	20.48	49.89	39.81	3.65
STG4-0.3-0.25	Pos.	31.44	7.73	50.5	19.5	42.93	29.76	3.85
	Neg.	46.95	12.54	57.7	25.3	49.05	38.83	3.1
	Ave.	39.2	10.14	54.1	22.4	45.99	34.3	3.48
STG4-0.5-0.25	Pos.	37.63	9.23	51.7	18.8	43.95	34.8	3.77
	Neg.	42.56	10.23	53.2	18.9	45.22	31.32	3.06
	Ave.	40.1	9.73	52.45	18.85	44.59	33.06	3.42

Table 5. *Cont.*

Specimen NO.	Direction	Yield Point		Peak Point		Failure Pint		$\mu = \Delta_\mu/\Delta_y$
		P_y/kN	Δ_y/mm	P_m/kN	Δ_m/mm	P_u/kN	Δ_u/mm	
STG4-0.7-0.25	Pos.	37.84	11.24	45.9	17.9	39.02	41.08	3.66
	Neg.	41.98	9.86	52.3	16.3	44.46	31.47	3.19
	Ave.	39.91	10.55	49.1	17.1	41.74	36.28	3.43
STG4-1-0.25	Pos.	32.48	9.3	46.5	17.9	39.53	33.55	3.61
	Neg.	40.85	10.3	50.8	17.9	43.18	31.22	3.03
	Ave.	36.67	9.8	48.65	17.9	41.36	32.39	3.32
STG4-0.5-0.05	Pos.	35.8	10.33	48.7	28.5	41.4	77.08	7.46
	Neg.	40.68	10.81	52.6	28	44.71	59.87	5.54
	Ave.	38.24	10.57	50.65	28.25	43.06	68.48	6.5
STG4-0.5-0.5	Pos.	29.81	7.83	42.5	17.1	36.13	23.48	3.0
	Neg.	41.46	9.61	56.4	16.7	47.94	23.84	2.48
	Ave.	35.64	8.72	49.45	16.9	42.04	23.66	2.74
STG6-0.5-0.25	Pos.	52.1	10.99	67.4	26.3	57.29	40.69	3.73
	Neg.	47.81	9.78	62.6	23.3	53.21	40.07	4.1
	Ave.	49.96	10.39	65	24.8	55.25	40.38	3.92
STM4-0-0.25	Pos.	43.45	10.49	55.1	23.7	46.84	39.65	3.78
	Neg.	46.99	10.56	57	17.5	48.45	40.29	3.81
	Ave.	45.22	10.53	56.05	20.6	47.65	39.97	3.8
STM4-0.5-0.25	Pos.	45.79	10.61	54.8	18	46.58	38.46	3.63
	Neg.	41.37	10.48	50.3	18.8	42.76	38.92	3.71
	Ave.	43.58	10.55	52.55	18.4	44.67	38.69	3.67
STM 4-1-0.25	Pos.	40.75	9.9	49.8	17.1	42.33	36.63	3.7
	Neg.	40.87	10.54	48.5	16.9	41.23	35.52	3.37
	Ave.	40.81	10.22	49.15	17	41.78	36.08	3.54

From Figure 10a and Table 5, it was clearly found that the peak load reduced with a higher replacement ratio of RBA, and compared with STG4-0-0.25, the bearing capacity of STG4-0.3-0.25, STG-0.5-0.25, STG4-0.7-0.25 and STG4-1-0.25 decreased by 9.48%, 11.25%, 16.92% and 17.68%, respectively. It was analyzed that due to the inherent flaw of RBA, the initial damage accumulated with the increase of RBA replacement ratio, and the negative effect caused by the inherent flaw became influential, leading to a more negative effect on the bearing capacity. Moreover, the difference in the failure mode was more evident since the confinement effect was weakened once yielding of the steel tube occurred. In Figure 10b, the increase of the steel tube thickness was beneficial for the initial stiffness and the peak load, while it had little influence on the degradation in behavior. The reason for this was that in the degrading stage, the confinement from steel tube was no longer effective due to the bulge of the steel tube. The bearing capacity of STG6-0.5-0.25 was increased by 23.98% compared with STG4-0.5-0.25, since a thicker steel tube provided better confinement to inner concrete, which in return provided favorable lateral support for the steel tube to prevent premature buckling under a small load. In Figure 10c, the influence on the bearing capacity was insignificant when the axial compression ratio was less than 0.25. The degradation in resistance of GRBACFST column was gentler under a small axial compression ratio. The applied axial load would result in a more serious P-Δ effect with a higher axial compression, leading to premature yielding or bulging of the steel tube; moreover, the inner concrete was also more prone to crack and crash. As in Figure 10d, it was concluded that the bearing capacity of composite columns was close when the only variable was cementitious material, while specimens GRBACFST columns always developed a relatively higher bearing capacity than specimens RBACFST columns. The result was comparable to the result in reference [47], and it was considered that the finer compactness of concrete was achieved during the hydration reaction with geopolymers.

3.4. Ductility

Ductility defined as the ratio between ultimate displacement corresponding to the load decreasing to less than 85% of peak load and yielding displacement was used to evaluate the plastic deformation capacity, and the results of ductility was also listed in Table 5. As listed, the ductility significantly decreased with axial compression ratio increasing, and the ductility decreased from 6.5 to 2.74, corresponding to axial compression ratio of 0.05 and 0.5. The reason that the confinement effect from steel tube was impaired with increasing of axial compression ratio, especially when the steel tube buckled. In terms of the RBA replacement ratio, the ductility of STG4-0.3-0.25, STG4-0.5-0.25, STG4-0.7-0.25 and STG4-1-0.25 decreased by 4.66%, 6.3%, 6.02% and 9.04%, respectively, compared with STG4-0-0.25, and the ductility of STM4-0.5-0.25 and STM4-1-0.25 was, respectively, 3.42% and 6.84% lower than that of STM4-0-0.25. With a larger proportion of RBA, the ductility was reduced, since the specimens was more likely to fail with the crash of inner concrete. Besides, the ductility of STG6-0.5-0.25 was 14.62% higher than that of STG4-0.5-0.25, because a thicker steel tube could provide a higher confinement effect and delay the loss of the interaction with inner concrete.

3.5. Degradation Characteristics

3.5.1. Stiffness Degradation

Stiffness degradation reflects the degradation process during cyclic loading. The secant stiffness was used to represent the stiffness for each loading cycle, defined as Equation (1), where P_i^+ and P_i^- are the peak load at the first cycle of each loading level, while Δ_i^+ and Δ_i^- are the corresponding displacement for P_i^+ and P_i^-:

$$K_i = \frac{|P_i^+| + |P_i^-|}{|\Delta_i^+| + |\Delta_i^-|} \quad (1)$$

Furthermore, the degradation coefficient τ was introduced, defined as the ratio of secant stiffness at the i^{th} loading level to the initial stiffness was introduced. Figure 11 exhibited the degradation characteristics curve τ-Δ/Δ_y for the proposed columns under different parameters.

As illustrated, the stiffness gradually degraded with an increase of Δ/Δ_y, but the degradation rate was reduced under large displacement. Generally, when Δ/Δ_y was less than 2.0, the influences of involved parameters on the stiffness degradation was not significant, but the stiffness degraded more quickly compared with the case when Δ/Δ_y was less than 3.0. It was analyzed that under a larger displacement, the damage of inner concrete accumulated and the confinement effect from steel tube was reduced due to the bulge of steel tube. The stiffness degradation was apparently affected by the axial compression ratio, since additional bending moment under larger displacement caused by P-Δ effect accelerated the failure process of GRBACFST columns. When Δ/Δ_y was small, the influence of the steel tube thickness on the stiffness degradation was insignificant; however, the contribution from thicker steel tube on the delay of stiffness degradation increased if Δ/Δ_y was larger than 2.0.

3.5.2. Strength Degradation

Strength degradation coefficient λ_j, calculated by Equation (2), was introduced to reflect the influence of loading cycles on the strength development under the same loading level, where P_j^1 and P_j^2 are the peak load at the first cycle and second cycle of jth loading level. The calculated result for the strength degradation coefficient curve λ_j-Δ/Δ_y is given in Figure 12.

$$\lambda_j = \frac{P_j^2}{P_j^1} \quad (2)$$

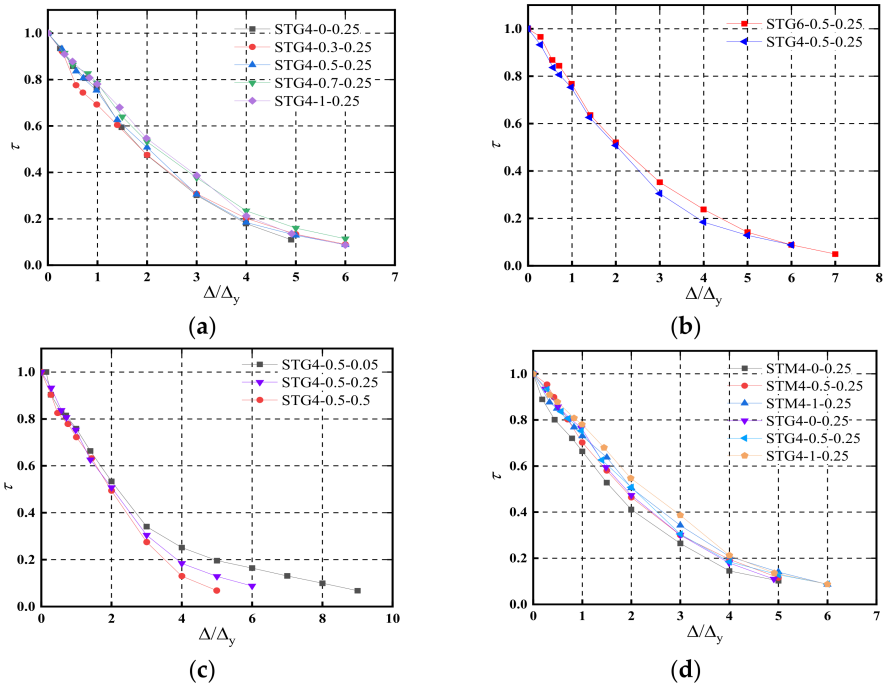

Figure 11. (**a**) Stiffness degradation coefficient curve τ-Δ/Δ_y for different replacement ratios of RBA; (**b**) stiffness degradation coefficient curve τ-Δ/Δ_y for different steel tube thicknesses; (**c**) stiffness degradation coefficient curve τ-Δ/Δ_y for different axial compression ratios; (**d**) stiffness degradation coefficient curve τ-Δ/Δ_y for different cementitious materials.

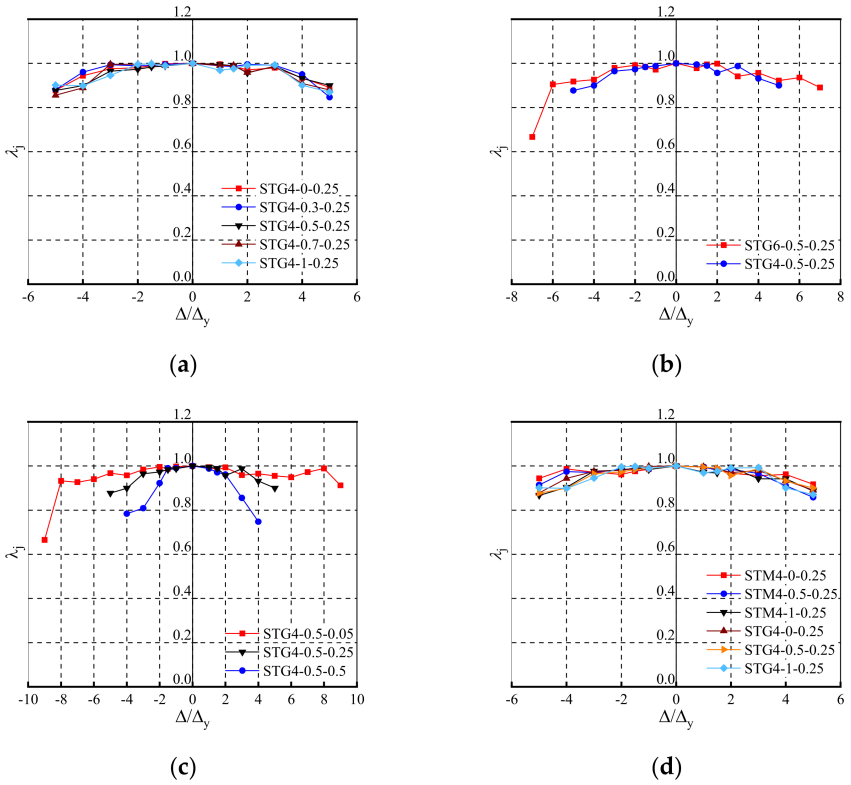

Figure 12. (**a**) Strength degradation coefficient curve λ_j-Δ/Δ_y for different replacement ratios of RBA; (**b**) strength degradation coefficient curve λ_j-Δ/Δ_y for different steel tube thicknesses; (**c**) strength degradation coefficient curve λ_j-Δ/Δ_y for different axial compression ratios; (**d**) strength degradation coefficient curve λ_j-Δ/Δ_y for different cementitious materials.

It could be seen that, except for the axial compression ratio, the influence of the other involved parameters on the strength degradation was not evident before Δ/Δ_y approached 3.0 (approximately corresponding to the peak point). This indicates that the tested columns remained in good condition as a whole and the cumulative damage was slight before reaching the peak load. From Figure 12a,d, the strength deteriorated with the displacement increasing, but the increase of RBA and the change of cementitious material did not affect the strength degradation under same deformation. From Figure 12b, the strength degradation for the specimen with a thicker steel tube was alleviated, since a thicker steel tube led to better improvement in mechanical behavior. Figure 12c showed the influence of the axial compression ratio, and it was clearly seen that the strength degradation was accelerated with a large axial compression ratio after yielding. This was also attributed to the P-Δ effect, leading to the concrete crush at the bottom of column under the largest bending moment and the degradation in strength.

3.6. Energy Dissipation

The influence of different parameters on the energy dissipation behavior is demonstrated in Figure 13. The energy dissipation capacities for tested specimens were similar during the initial stage (Δ/Δ_y less than 2.0). The incorporation of RBA had a negative effect on the energy dissipation (as in Figure 13a), mainly due to the reduction in bearing capacity. However, the increase of RBA replacement ratio did not impact the energy dissipation a lot. From Figure 13b, specimen STC6-0.5-0.25 exhibited higher energy dissipation capacity than STC4-0.5-0.25 and the ultimate displacement was also larger. This was because the bearing capacity and deformation capacity were enhanced, owing to better confinement effect from a thicker steel tube. The effect of the axial compression ratio on the energy dissipation behavior was not significant when the axial compression ratio was small. However, a larger axial compression ratio might reduce the energy dissipation capacity, since it resulted in more serious degradation in bearing capacity. In Figure 13d, it was concluded that the replacement of OPC with geopolymer did not affect the energy dissipation behavior, which was mainly determined by the plastic behavior of the proposed columns.

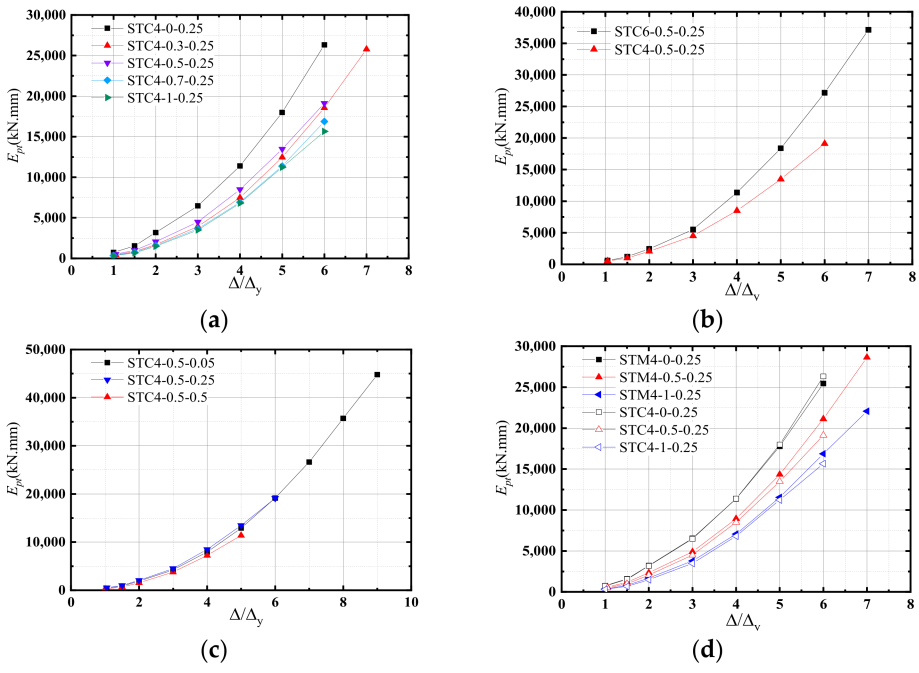

Figure 13. (**a**) Strength degradation coefficient curve λ_j-Δ/Δ_y for different replacement ratios of RBA; (**b**) strength degradation coefficient curve λ_j-Δ/Δ_y for different steel tube thicknesses; (**c**) strength degradation coefficient curve λ_j-Δ/Δ_y for different axial compression ratios; (**d**) strength degradation coefficient curve λ_j-Δ/Δ_y for different cementitious materials.

3.7. Strain Analysis

As presented in Figure 3, strain gauges #1 to #3 were used to demonstrate the longitudinal strain development at different location along column height, while strain gauges #2, 9, 16 and 23 were selected to elaborate the development of longitudinal strain at different sides of square steel tube. Strain gauges #8, 14, 22, 28 were used to illustrate the transverse strain, which could be used to reflect the failure process of inner concrete. The hysteresis curves P-ε_y (longitudinal direction) and P-ε_x (transverse direction) for STG4-0.5-0.25 were given in Figures 14 and 15 as an example to elaborate the strain development.

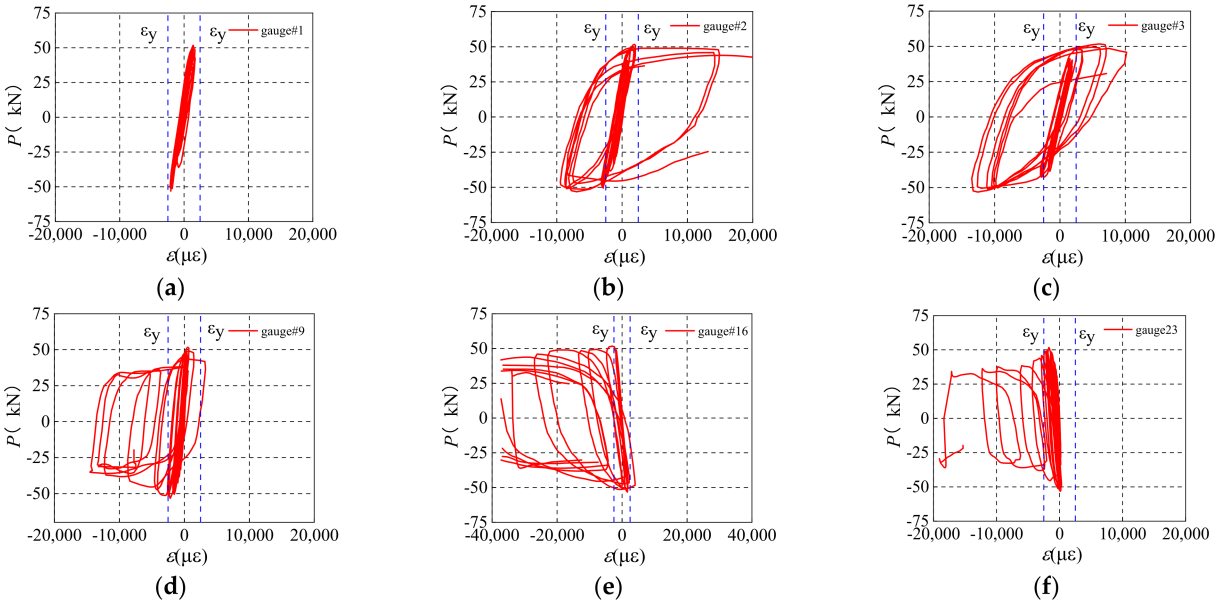

Figure 14. (**a**) P-ε_y hysteresis curve for STG4-0.5-0.25 of gauge#1; (**b**) P-ε_y hysteresis curve for STG4-0.5-0.25 of gauge#2; (**c**) P-ε_y hysteresis curve for STG4-0.5-0.25 of gauge#3; (**d**) P-ε_y hysteresis curve for STG4-0.5-0.25 of gauge#9; (**e**) P-ε_y hysteresis curve for STG4-0.5-0.25 of gauge#16; (**f**) P-ε_y hysteresis curve for STG4-0.5-0.25 of gauge#23.

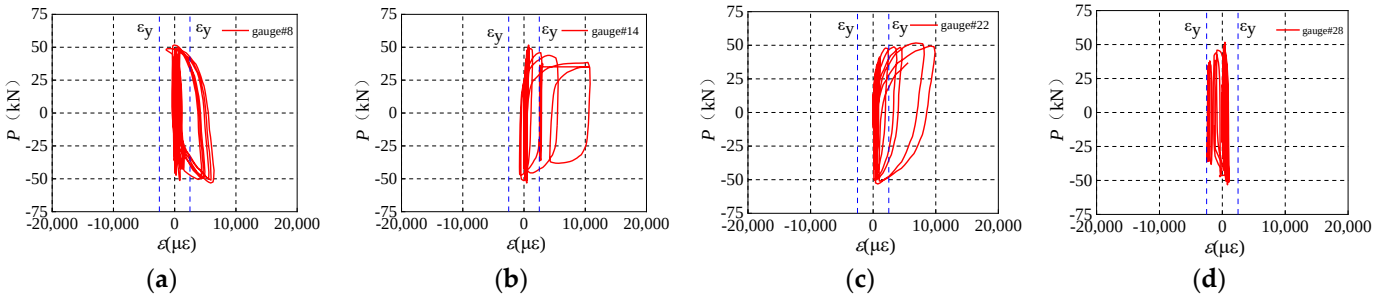

Figure 15. (**a**) P-ε_x hysteresis curve for STG4-0.5-0.25 of gauge#8; (**b**) P-ε_x hysteresis curve for STG4-0.5-0.25 of gauge#14; (**c**) P-ε_x hysteresis curve for STG4-0.5-0.25 of gauge#22; (**d**) P-ε_x hysteresis curve for STG4-0.5-0.25 of gauge#28.

As seen in Figure 14, the development of P-ε_y hysteresis curve was similar with load-displacement hysteresis behavior in Figures 8 and 9. During the whole loading process, the strain for gauge #1 was less than the yield strength due to the smaller bending moment and stable behavior of the steel tube without local buckling. It could be inferred that strain gauge #1 did not locate in the plastic hinge region. Strain gauges in side A and C (strain gauge #2 and #16) were larger than that in Side B and D (strain gauge #9 and #23), and this result coincided with the observation that the deformation in Side A and C was more serious than that in Side B and D. Once the steel tube yielded, the strain developed quickly

with an increasing load. It should be noted that under larger deformation, strain gauges located in the region with serious bulge or buckling would fail and the measured strain data lost accuracy.

It was known that the transverse strain was mainly induced by the interaction between the steel tube and inner concrete. Therefore, the transverse strain was small at the initial loading stage, indicating that the confinement to inner concrete was slight before buckling, as shown in Figure 15. However, under larger deformation, the confinement to the concrete was reduced due to the buckling of steel tube, the inner concrete would expand transversely and led to the rapid increase of transverse strain. Besides, the transverse strain was generally in tension since large unrecovered residual deformation of steel tube occurred due to the bulge. Because of the serious bulge in the region at column root or the rupture of steel tube, some of the strains gauges located in or adjacent to the region with serious bulge either failed or fall off, leading to the lack of strain date in the late loading stage.

4. Conclusions

A new type of GRBACFST composite column was proposed to improve the environmental sustainability of CFST column and enhance the reuse efficiency of construction waste and industrial waste. The cyclic behaviors of GRBACFST column were studied experimentally and the influences of the replacement ratio of RBA, steel tube thickness, axial compression ratio and cementitious material types were discussed. Based on the test results, some important conclusions could be summarized as follows.

(1) The proposed GRBACFST column could develop good hysteretic behavior that was comparable to conventional CFST column, in terms of failure process, failure mode and deformation capacity. The plastic hinge always formed at the bottom region of column and the GRBACFST column failed with bulge of steel tube or rupture of steel tube at the corner. The inner GRBAC at the region with serious local buckling occurred was found with serious crush.

(2) The hysteretic curves for proposed GRBACFST columns were full without an evident pinching effect and excellent deformation capacity. The incorporation of RBA and increase of axial compression ratio imposed an evidently negative effect on the bearing capacity, while a thicker steel tube was beneficial. The hysteretic behavior was analogous for tested specimens with different cementitious material.

(3) The mechanical behavior was similar for all tested columns during the initial stage. However, once the steel tube yielded or buckled, the deference in the degradation stage was obvious. Specimens with larger RBA replacement ratio, higher axial compression ratio and thinner steel tube developed a serious degradation in mechanical behavior.

(4) The confinement effect from steel tube could effectively offset the drawbacks of crushed brick aggregate, especially for cases with higher replacement ratios of RBA or under larger deformation. A thicker steel tube could improve the failure process of proposed GRBACFST column and benefit the bearing capacity, ductility as well as energy dissipation ability.

(5) The hysteretic behavior was not sensitive to the change of cementitious material, and the geopolymers could serve as an effective alternative to the OPC as an eco-friendly binder for concrete. It was feasible to develop a green building material with industrial waste and construction waste, effectively dealing with the shortage of natural resources and environmental issue.

Author Contributions: Conceptualization, Y.N. and R.L.; Data curation, Y.C. and X.L.; Investigation, Y.C.; Methodology, Y.N.; Project administration, R.L.; Software, X.L.; Supervision, R.L.; Writing—original draft, Y.C.; Writing—review and editing, Y.N. All authors have read and agreed to the published version of the manuscript.

Funding: This research was funded by the University-Industry Cooperation Project of Fujian Province (Grant No. 2021Y4018) and Fujian Provincial Finance Department (GY-Z21005).

Institutional Review Board Statement: Not applicable.

Informed Consent Statement: Not applicable.

Data Availability Statement: Not applicable.

Conflicts of Interest: The authors declare no conflict of interest.

References

1. Ding, T.; Xiao, J.; Tam, V.W. A closed-loop life cycle assessment of recycled aggregate concrete utilization in China. *Waste Manag.* **2016**, *56*, 367–375. [CrossRef] [PubMed]
2. Zhang, C.; Hu, M.; Dong, L.; Xiang, P.; Zhang, Q.; Wu, J.; Li, B.; Shi, S. Co-benefits of urban concrete recycling on the mitigation of greenhouse gas emissions and land use change: A case in Chongqing metropolis, China. *J. Clean. Prod.* **2018**, *201*, 481–498. [CrossRef]
3. Imbabi, M.S.; Carrigan, C.; McKenna, S. Trends and developments in green cement and concrete technology. *Int. J. Sustain. Built Environ.* **2012**, *1*, 194–216. [CrossRef]
4. Andrew, R.M. Global CO2 emissions from cement production, 1928–2018. *Earth Syst. Sci. Data* **2019**, *11*, 1675–1710. [CrossRef]
5. Marinković, S.B.; Ignjatović, I.S.; Radonjanin, V.S.; Malešev, M.M. Recycled aggregate concrete for structural use–an overview of technologies, properties and applications. *Innov. Mater. Tech. Concr. Constr.* **2012**, 115–130. [CrossRef]
6. Lotfi, S.; Eggimann, M.; Wagner, E.; Mróz, R.; Deja, J. Performance of recycled aggregate concrete based on a new concrete recycling technology. *Constr. Build. Mater.* **2015**, *95*, 243–256. [CrossRef]
7. Liu, F.; Feng, W.; Xiong, Z.; Tu, G.; Li, L. Static and impact behaviour of recycled aggregate concrete under daily temperature variations. *J. Clean. Prod.* **2018**, *191*, 283–296. [CrossRef]
8. Li, W.; Luo, Z.; Long, C.; Wu, C.; Duan, W.H.; Shah, S.P. Effects of nanoparticle on the dynamic behaviors of recycled aggregate concrete under impact loading. *Mater. Des.* **2016**, *112*, 58–66. [CrossRef]
9. Liu, B.; Feng, C.; Deng, Z. Shear behavior of three types of recycled aggregate concrete. *Constr. Build. Mater.* **2019**, *217*, 557–572. [CrossRef]
10. Gales, J.; Parker, T.; Cree, D.; Green, M. Fire performance of sustainable recycled concrete aggregates: Mechanical properties at elevated temperatures and current research needs. *Fire Technol.* **2016**, *52*, 817–845. [CrossRef]
11. Pliya, P.; Cree, D.; Hajiloo, H.; Beaucour, A.-L.; Green, M.F.; Noumowé, A. High-strength concrete containing recycled coarse aggregate subjected to elevated temperatures. *Fire Technol.* **2019**, *55*, 1477–1494. [CrossRef]
12. Guo, H.; Shi, C.; Guan, X.; Zhu, J.; Ding, Y.; Ling, T.C.; Zhao, H.; Wang, Y. Durability of recycled aggregate concrete–A review. *Cem. Concr. Compos.* **2018**, *89*, 251–259. [CrossRef]
13. Domingo-Cabo, A.; Lázaro, C.; López-Gayarre, F.; Serrano-López, M.A.; Serna, P.; Castaño-Tabares, J.O. Creep and shrinkage of recycled aggregate concrete. *Constr. Build. Mater.* **2009**, *23*, 2545–2553. [CrossRef]
14. Seara-Paz, S.; González-Fonteboa, B.; Martínez-Abella, F.; González-Taboada, I. Time-dependent behaviour of structural concrete made with recycled coarse aggregates. Creep and shrinkage. *Constr. Build. Mater.* **2016**, *122*, 95–109. [CrossRef]
15. Xiao, J.; Poon, C.S.; Wang, Y.; Zhao, Y.; Ding, T.; Geng, Y.; Ye, T.; Li, L. Fundamental behaviour of recycled aggregate concrete–Overview I: Strength and deformation. *Mag. Concr. Res.* **2022**, *74*, 1–12. [CrossRef]
16. Tabsh, S.W.; Abdelfatah, A.S. Influence of recycled concrete aggregates on strength properties of concrete. *Constr. Build. Mater.* **2009**, *23*, 1163–1167. [CrossRef]
17. Medina, C.; Zhu, W.; Howind, T.; de Rojas, M.I.S.; Frías, M. Influence of mixed recycled aggregate on the physical-mechanical properties of recycled concrete. *J. Clean. Prod.* **2014**, *68*, 216–225. [CrossRef]
18. Formoso, C.T.; Soibelman, L.; De Cesare, C.; Isatto, E.L. Material waste in building industry: Main causes and prevention. *J. Constr. Eng. Manag.* **2002**, *128*, 316–325. [CrossRef]
19. Mohammed, T.U.; Hasnat, A.; Awal, M.A.; Bosunia, S.Z. Recycling of brick aggregate concrete as coarse aggregate. *J. Mater. Civ. Eng.* **2015**, *27*, B4014005. [CrossRef]
20. He, Z.; Shen, A.; Wang, W.; Zuo, X.; Wu, J. Evaluation and optimization of various treatment methods for enhancing the properties of brick-concrete recycled coarse aggregate. *J. Adhes. Sci. Technol.* **2021**, *36*, 1–21. [CrossRef]
21. Younis, K.H.; Pilakoutas, K. Strength prediction model and methods for improving recycled aggregate concrete. *Constr. Build. Mater.* **2013**, *49*, 688–701. [CrossRef]
22. Yang, J.; Shaban, W.M.; Elbaz, K.; Thomas, B.S.; Xie, J.; Li, L. Properties of concrete containing strengthened crushed brick aggregate by pozzolan slurry. *Constr. Build. Mater.* **2020**, *247*, 118612. [CrossRef]
23. Junak, J.; Sicakova, A.; Junakova, N. Surface treatments of recycled brick aggregate and their influence on selected properties of concrete. Proceedings of Advances in Environmental Engineering, Virtual Conference, Czech Republic, 25–26 November 2021; 2021; Volume 900, p. 12014. [CrossRef]
24. Islam, M.; Siddique, M.A.A. Behavior of low grade steel fiber reinforced concrete made with fresh and recycled brick aggregates. *Adv. Civ. Eng.* **2017**, *2017*, 1812363. [CrossRef]
25. Tam, V.W.; Soomro, M.; Evangelista AC, J.; Haddad, A. Deformation and permeability of recycled aggregate concrete-A comprehensive review. *J. Build. Eng.* **2021**, *44*, 103393. [CrossRef]

26. Singh, B.; Ishwarya, G.; Gupta, M.; Bhattacharyya, S. Geopolymer concrete: A review of some recent developments. *Constr. Build. Mater.* **2015**, *85*, 78–90. [CrossRef]
27. Almutairi, A.L.; Tayeh, B.A.; Adesina, A.; Isleem, H.F.; Zeyad, A.M. Potential applications of geopolymer concrete in construction: A review. *Case Stud. Constr. Mater.* **2021**, *15*, e00733. [CrossRef]
28. Villaquirán-Caicedo, M.A. Studying different silica sources for preparation of alternative waterglass used in preparation of binary geopolymer binders from metakaolin/boiler slag. *Constr. Build. Mater.* **2019**, *227*, 116621. [CrossRef]
29. Xie, T.; Ozbakkaloglu, T. Behavior of low-calcium fly and bottom ash-based geopolymer concrete cured at ambient temperature. *Ceram. Int.* **2015**, *41*, 5945–5958. [CrossRef]
30. Nuaklong, P.; Sata, V.; Chindaprasirt, P. Influence of recycled aggregate on fly ash geopolymer concrete properties. *J. Clean. Prod.* **2016**, *112*, 2300–2307. [CrossRef]
31. Hu, Y.; Tang, Z.; Li, W.; Li, Y.; Tam, V.W. Physical-mechanical properties of fly ash/GGBFS geopolymer composites with recycled aggregates. *Constr. Build. Mater.* **2019**, *226*, 139–151. [CrossRef]
32. Xie, J.; Wang, J.; Rao, R.; Wang, C.; Fang, C. Effects of combined usage of GGBS and fly ash on workability and mechanical properties of alkali activated geopolymer concrete with recycled aggregate. *Compos. Part B Eng.* **2019**, *164*, 179–190. [CrossRef]
33. Tang, Z.; Li, W.; Tam, V.W.; Luo, Z. Investigation on dynamic mechanical properties of fly ash/slag-based geopolymeric recycled aggregate concrete. *Compos. Part B Eng.* **2020**, *185*, 107776. [CrossRef]
34. Liang, Y.-C.; Ye, Z.-M.; Vernerey, F.; Xi, Y. Development of processing methods to improve strength of concrete with 100% recycled coarse aggregate. *J. Mater. Civ. Eng.* **2015**, *27*, 04014163. [CrossRef]
35. Tang, Z.; Hu, Y.; Tam, V.W.; Li, W. Uniaxial compressive behaviors of fly ash/slag-based geopolymeric concrete with recycled aggregates. *Cem. Concr. Compos.* **2019**, *104*, 103375. [CrossRef]
36. Chen, Z.; Xu, J.; Chen, Y.; Lui, E.M. Recycling and reuse of construction and demolition waste in concrete-filled steel tubes: A review. *Constr. Build. Mater.* **2016**, *126*, 641–660. [CrossRef]
37. Xu, J.-J.; Chen, Z.-P.; Xiao, Y.; Demartino, C.; Wang, J.-H. Recycled aggregate concrete in FRP-confined columns: A review of experimental results. *Compos. Struct.* **2017**, *174*, 277–291. [CrossRef]
38. Tang, Z.; Li, W.; Tam, V.W.; Yan, L. Mechanical behaviors of CFRP-confined sustainable geopolymeric recycled aggregate concrete under both static and cyclic compressions. *Compos. Struct.* **2020**, *252*, 112750. [CrossRef]
39. Dey, T.; Das, C.S.; Mishra, N. Behaviour of confined recycled aggregate concrete under compressive loading: An experimental investigation. *J. Build. Eng.* **2020**, *32*, 101825. [CrossRef]
40. Zhao, J.L.; Yu, T.; Teng, J.G. Stress-strain behavior of FRP-confined recycled aggregate concrete. *J. Compos. Constr.* **2015**, *19*, 4014054. [CrossRef]
41. Xie, T.; Ozbakkaloglu, T. Behavior of recycled aggregate concrete-filled basalt and carbon FRP tubes. *Constr. Build. Mater.* **2016**, *105*, 132–143. [CrossRef]
42. Tang, Y.-C.; Li, L.-J.; Feng, W.-X.; Liu, F.; Liao, B. Seismic performance of recycled aggregate concrete–filled steel tube columns. *J. Constr. Steel Res.* **2017**, *133*, 112–124. [CrossRef]
43. Zhang, X.; Gao, X. The hysteretic behavior of recycled aggregate concrete-filled square steel tube columns. *Eng. Struct.* **2019**, *198*, 109523. [CrossRef]
44. *GB/T228.1-2010*; Metallic Materials-Tensile Testing Part 1: Method of Test at Room Temperature. Standards Press of China: Beijing, China, 2010. (In Chinese)
45. *GB/T50081-2019*; Standard for Test Methods of Concrete Physical and Mechanical Properties. China Architecture & Building Press: Beijing, China, 2019. (In Chinese)
46. Krawinkler, H.; Applied Technology Council. *Guidelines for Cyclic Seismic Testing of Components of Steel Structures*; Applied Technology Council ATC-24: Redwood City, CA, USA.
47. Xie, J.; Wang, J.; Zhang, B.; Fang, C.; Li, L. Physicochemical properties of alkali activated GGBS and fly ash geopolymeric recycled concrete. *Constr. Build. Mater.* **2019**, *204*, 384–398. [CrossRef]